Measurement and analysis of excitation functions of the residues from $^{12}C + ^{89}Y$: A major production route for ^{97}Ru

Amit Chauhan and Moumita Maiti*
Department of Physics, Indian Institute of Technology Roorkee, Roorkee-247667, Uttarakhand, India

Susanta Lahiri
Saha Institute of Nuclear Physics, 1/AF Bidhannagar, Kolkata-700064, India

(Received 28 April 2019; published 13 June 2019)

Background: ^{97}Ru, a good hepatobiliary agent, is used in delayed investigations, diagnostic and therapeutic purposes, due to its favorable physicochemical properties. Various experimental studies have been carried out to investigate its production and chemical separation. However, in the interest of the subject, a lot of investigation is still required to identify the suitable routes for its optimum production, particularly for heavy-ion reactions, and to understand the reaction mechanisms.

Purpose: Measurement and analysis of excitation function of the residues from the $^{12}C+^{89}Y$ reaction at the low-energy region and to estimate the cross-section of ^{97}Ru expected to be produced through the direct channel, and indirectly via the decay of its short-lived precursors ^{97g,97m}Rh.

Method: Thin ^{89}Y foils backed by aluminium were bombarded by the $^{12}C^{6+}$ beam within 40–75 MeV energy range. The excitation functions of the residues have been measured with the help of off-line γ-ray spectroscopy. Experimental cross-sections are compared with the various reaction models to understand the reaction mechanism involved in the production of residual radionuclides.

Results: The measured cross-sections of ^{97}Ru, $^{98,97m+g,96}$Rh, ^{96,95,94,93}Tc, and ^{93m}Mo radionuclides show reasonably good agreement with the calculations based on the equilibrium (EQ) and preequilibrium (PEQ) models. The contribution of PEQ emissions is observed in the $3n$ and αxn ($x = 1, 2$) channels.

Conclusion: Comparative analysis of the residual cross-sections demonstrates the dominance of compound nuclear process in the energy range considered. The measured cumulative production cross-section of ^{97}Ru is maximum, ~850 mb, at 66.6 MeV. The detailed analysis presented in this article would help to optimize the production parameters for ^{97}Ru and also to understand the reliability of the theoretical models.

DOI: 10.1103/PhysRevC.99.064609

I. INTRODUCTION

Even though reactors are commonly used for the production of medical radionuclides to achieve high yield, cyclotron produced positron emitters have found a variety of applications in the field [1,2]. Thus, the production of neutron-deficient radionuclide is a subject of interest from several decades. As far as the application of radionuclides is concerned, both neutron-deficient and neutron-rich radionuclides could be used for a specific application if they suffice the purpose. However, the highly specific activity of the radionuclides, which could be achieved in an accelerator production route followed by the chemical separation, is the requirement in nuclear medicine. As an example, chelated compounds such as ^{169}Yb/^{99m}Tc/^{111}In-DTPA (diethylenetriaminepentaacetic acid) are adopted well for cisternography [3–5]. Studies show that ^{169}Yb delivers a higher dose due to its long half-life of 32 days, whereas the life of ^{99m}Tc ($T_{1/2}$ = 6.04 h) is too short for the evaluation of adult hydrocephalus during delayed (48–72 h) scanning. ^{111}In-DTPA, having $T_{1/2}$ = 2.80 d for ^{111}In, acts well to provide adequate quality control and also permits prolonged studies due to its suitable physical characteristics, but it emits Auger electrons within a range of nanometer to micrometer, which damage DNA (deoxyribonucleic acid). Preclinical studies show that it binds to cytoplasmic components and cell membrane during decay.

In this scenario, ^{97}Ru (2.83 d) could be considered as a potential alternative due to its excellent chemical and physical properties. It decays through electron capture (without β-emission) followed by the emission of 215.70 keV (85.62%) and 324.49 keV(10.79%) γ-rays, which offer better diagnostic imaging, lower radiation dose to the tissue, and it also works as a promising therapeutic agent [6,7]. The radionuclide production technology today is, therefore, an integral part of modern nuclear medicine and its future prospects.

^{97}Ru radionuclides had been produced through light-ion-induced (p, ^{3,4}He, etc.) reactions, ^{nat}Mo(^{4,3}He, xn)^{97}Ru, ^{nat}Rh(p, $2p5n$)^{97}Ru, ^{99}Tc(p, $3n$)^{97}Ru, by several groups [8–11]. Besides this, production of ^{97}Ru has also been probed through the heavy-ion (^{7}Li, ^{11}B, ^{12}C)-induced reactions on ^{93}Nb, ^{89}Y, and ^{nat}Mo [12–20] by our group, where focus

*moumifph@iitr.ac.in; moumifph@gmail.com

was mostly on the development of efficient radiochemical separation for ^{97}Ru. Cross-sections of the residues including ^{97}Ru were also reported for ^{7}Li+^{93}Nb/^{nat}Mo, and ^{11}B+^{89}Y/^{93}Nb [17–20]. Although light-ion reactions are preferred to achieve substantial yield for the desired radionuclides, some heavy-ion reactions may offer considerable yield to conduct test experiments at the laboratory scale. In this endeavor, we report a new measurement of cross-sections of the residues produced in the ^{12}C+^{89}Y reaction in the low-energy range.

Apart from the application, understanding of the heavy-ion reaction mechanisms such as threshold anomaly around the barrier, breakup fusion, preequilibrium (PEQ) process, quasielastic, direct effects, and transfer reaction, etc., is important; hence, more investigation is required over a wide energy range. Although the existence of the PEQ process is well established in the light-ion-induced reactions, the interplay between PEQ and compound nuclear or equilibrium (EQ) mechanism in heavy-ion-induced reactions is complex in nature, yet it was explored by several groups at higher energies, within 10–20 MeV/nucleon [21–25]. However, the evidence of PEQ emissions in 3n channel from several reactions, ^{12}C+^{128}Te/^{169}Tm and ^{16}O + ^{159}Tb/^{169}Tm/^{181}Ta, has been reported at relatively low energies, below 10 MeV/nucleon [26]. In general, PEQ emission is found to depend strongly on the projectile energy. Estimation of PEQ fraction is a measure of the relative strength of the PEQ component that leads to the formation of a residue. The trustworthiness of nuclear reaction models is also supported by the presence of PEQ emissions to the formation of isomers.

Study of isomeric cross-section ratio (ICR) of the residual nucleus at different energies is also important to understand the angular momentum effects, spin distribution, and channel effects for the formation of isomeric pairs in a nuclear reaction. Vandenbosch *et al.* [27] had investigated the formation of high spin isomer with an increase in the projectile energy and deduced the effect of nuclear-level density on the angular momentum. ICR for an isomeric pair strongly depends on the level scheme, branching ratios of the known levels of the radionuclide and on the energy difference between the levels. It is also observed that different reactions produce atypical angular momentum distributions of the compound nucleus, resulting in different ICR at the same excitation of the compound nucleus. Apart from this, ICRs also depend on the PEQ angular distribution and on the spin cutoff parameter for EQ emissions. Hence, it is rather difficult to estimate the cross-sections for the formation of isomeric states [28–30]. The study of ICR is, therefore, important to have enough knowledge to understand the nuclear reaction mechanism and models.

In the late '90s, Kumar *et al.* [31] reported the excitation functions for radioactive isotopes produced in the energy range 70–87 MeV and extended the interpretation of recoil range distribution at 84 MeV for ^{12}C-induced reaction on ^{89}Y target. Later, Mukherjee *et al.* reported the isomeric cross-section ratio of ^{99}Rh from the ^{12}C+^{89}Y system between 30 and 45 MeV and showed that the average angular momentum decreases with decreasing beam energy until the fusion barrier is reached [32]. In view of this, we have explored the ^{12}C-induced reaction on ^{89}Y target within the 40–75 MeV energy range.

The present work aims for the following:

(1) Measurement of cross-sections of the residues from ^{12}C+^{89}Y reaction.
(2) Cross-section analysis for ^{97}Ru.
(3) Study of reaction mechanisms, ICR- and PEQ-fraction analysis.

Section II depicts the experimental details. Section III presents the results and discussion, and Sec. IV summarizes the report.

II. EXPERIMENTAL DETAILS

The experiment was performed at the BARC-TIFR Pelletron accelerator facility, Mumbai, India. The natural yttrium (^{89}Y) foils having the thickness of 1.8–2.0 mg/cm^2 and the aluminium (Al) foils of thickness 1.5 mg/cm^2 were prepared by proper rolling. The foils were mounted on the Al-rings of 12 mm inner and 22 mm outer diameter which resembles the geometry of the irradiation chamber closely. A stack of Y-Al foils, with each Y foil backed by an Al-catcher, was bombarded by ^{12}C^{6+} beam within the energy range between 40–75 MeV. The backing Al-foil fulfills the demand of energy degradation and also acts as a catcher for the evaporation residues along the beam direction. A total of five such Y-Al foil stacks were irradiated with a slight overlap in energy. Assuming the beam intensity is steady, the energy degradation through the target and catcher foil is estimated by the stopping and range of ions in matter (SRIM) code [33]. The total charge during irradiation was collected on a Faraday cup placed behind the assembly, and the duration of irradiation was varied from 1 to 3 h according to the half-lives and decay profile of the products. After the end-of-bombardment (EOB), each Y–Al foil combination was assayed by the γ-ray spectrometry using a high purity germanium detector with the help of GENIE-2K software. The efficiency calibration of the detector was done by using a standard γ-ray source, ^{152}Eu, of known activity. The energy resolution of the detector was 2.0 keV at the 1332 keV photo-peak of ^{60}Co. Assuming steady beam intensity, a systematic error introduced due to the use of multiple foils is neglected. The yield Y_r of the r^{th} evaporation residue after the EOB is calculated using

$$Y_r = C(E_r)e^{\lambda_r t_c}[\varepsilon_\gamma I_\gamma]^{-1}. \quad (1)$$

The cross-section of the evaporation residue $\sigma_r(E)$ at an incident energy E is obtained from

$$Y_r = \sigma_r(E) I_b \rho_f t_f (1 - e^{-\lambda_r t_m})(1 - e^{-\lambda_r t_i})\lambda_r^{-1}, \quad (2)$$

where $C(E_r)$ is the net counts under the photo-peak area; ε_γ and I_γ are the detection efficiency of the HPGe-detector and branching intensity of the characteristic γ ray, respectively, of the evaporation residue. ρ_f is the atomic density of the target foil; t_f is the thickness of target foil; λ_r is the decay constant; I_b is the beam intensity of projectile; t_i, t_c, and t_m are the irradiation, cooling, and counting times, respectively. To calculate the production cross-sections of the evaporation residue, the nuclear spectroscopic data are enlisted in Table I.

TABLE I. Spectroscopic data of the evaporation residues [34]. The γ-rays marked in bold are used in the calculation.

Nuclides (J^{π})	Half-life	Decay mode (%)	Eγ (keV) [Iγ(%)]	Reactions	E_{th}[a] (MeV)
^{98}Rh (2^+)	8.72 min	ϵ[b]+β^+ (100)	**652.6 [97.0]**	^{89}Y (^{12}C,3n)	32.6
			1164.3 [4.9]		
^{97g}Rh ($9/2^+$)	30.7 min	$\epsilon+\beta^+$ (100)	421.55 [74.6]	^{89}Y (^{12}C,4n)	42.4
			840.13 [12.0]		
^{97m}Rh ($1/2^-$)	46.2 min	$\epsilon+\beta^+$ (94.4)	**189.21 [48.5]**	^{89}Y (^{12}C,4n)	42.4
		IT[c] (5.6)	421.55 [12.7]		
			527.85 [8.3]		
^{96}Rh (6^+)	9.9 min	$\epsilon+\beta^+$ (100)	631.73 [74.5]	^{89}Y (^{12}C,5n)	54.9
			685.47 [95.7]		
			832.52 [100.0]		
^{97}Ru ($5/2^+$)	2.83 d	ϵ (100)	**215.70 [85.6]**	^{89}Y (^{12}C,p3n)	37.5
			324.49 [10.8]		
^{96}Tc (7^+)	4.28 d	$\epsilon+\beta^+$ (100)	**778.22 [99.8]**	^{89}Y (^{12}C, αn)	14.0
			849.86 [98.0]		
^{95}Tc ($9/2^+$)	20.0 h	$\epsilon+\beta^+$ (100)	**765.78 [93.8]**	^{89}Y (^{12}C, α2n)	22.9
			1073.71 [3.7]		
^{94}Tc (7^+)	293 min	$\epsilon+\beta^+$ (100)	**702.67 [99.6]**	^{89}Y (^{12}C, α3n)	34.3
			849.74 [95.7]		
			871.05 [99.9]		
^{93}Tc ($9/2^+$)	2.75 h	$\epsilon+\beta^+$ (100)	**1362.94 [66.2]**	^{89}Y (^{12}C, α4n)	44.0
			1477.14 [8.7]		
			1520.28 [24.4]		
^{93m}Mo ($21/2^+$)	6.85 h	IT (99.88)	**263.04 [57.4]**	^{89}Y (^{12}C, αp3n)	39.5
		$\epsilon+\beta^+$ (0.12)	684.69 [99.9]		
			1477.13 [99.1]		

[a]E_{th} represents threshold energy
[b]ϵ represents electron capture decay
[c]IT represents isomeric transition

During the cross-section measurement, uncertainties may arise due to (a) inaccuracy in determination of the foil thickness (∼2–3%), (b) inaccuracy in efficiency calibration of the detector (∼0.1–1%), (c) uncertainty in the projectile beam current measurement (∼6–7%), and (d) error due to counting statistics (∼6–7%). The error due to degradation of energy (Straggling effects) of the beam in the successive foils and the branching ratio of characteristic γ rays have been presumed as comparatively small in the present case [35–39].

III. RESULTS AND DISCUSSION

A. Theoretical analysis

The nuclear reaction mechanism can be broadly classified into three categories, namely, EQ, PEQ, and direct (DIR). In this article, an effort has been made to explain the measured cross-section data of the residues from the ^{12}C+^{89}Y reaction within the energy range 40–75 MeV using the EQ and PEQ reaction models. Statistical code PACE4, projection-angular momentum-coupled-evaporation [40], uses a Monte Carlo method for coupling angular momentum of the highly excited compound nucleus. The Monte Carlo procedure is used to determine the sequential decays by the Hauser-Feshbach (HF) formalism [41]. It provides the correlation between particles and γ rays, the angular distribution of particles. The fission is a decay mode which was added by a rotating liquid drop barrier routine. The code is implemented in the LISE++ tools to plot the calculated cross-sections, recommended a database for binding energy calculations, and fusion cross-section calculation below the Coulomb barrier using the quantum mechanical approach. A trace-back feature is also included which enables the determination of the decay chains and the region of the E-J plane leading to specific nuclei. During the first step of de-excitation, transmission coefficient for light particle evaporation such as neutron, proton, α particle, etc., is obtained by full optical model calculation. For the heavy ions, the Bass algorithm [42] is used to estimate complete fusion cross-section and to measure the evaporation residues. The Gilbert-Cameron formalism is accounted for the level density with parameter $a = A/9$, where A is the total number of nucleons in the compound nucleus, the ratio a_f/a_n is assumed unity. The code employs only the EQ reaction mechanism and does not consider PEQ processes.

EMPIRE3.2 accounts for the EQ, PEQ, and DIR processes. The full-featured HF model has been used with a mean free path multiplier 1.5 with exact angular momentum and parity coupling for compound nuclear process [43]. It includes γ cascade and width fluctuations to describe the decay process of the excited nucleus. The simplified coupled channel calculations (CCFULL) is implemented for fusion processes of heavy-ion-induced reactions. The exciton model (EM) based upon the solution of the master equation proposed by Cline and Ribansky is adopted to predict the PEQ [44,45]

TABLE II. Cross-section (mb) of evaporation residues at different incident energies

Energy	Cross − section(mb)									
(MeV)	^{98}Rh	^{97g}Rh	^{97m}Rh	^{96}Rh	^{97}Rh$_{cum}$	^{96}Tc	^{95}Tc	^{94}Tc	^{93}Tc	^{93m}Mo
41.1	86.2 ± 11.1				5.7 ± 3.4	25.7 ± 6.3	20.8 ± 2.5	0.4 ± 0.3		
48.2	218.6 ± 51.8	6.4 ± 2.1	1.3 ± 0.4		19.2 ± 4.1	26.6 ± 8.2	93.9 ± 7.8	0.8 ± 0.3		
50.9	298.9 ± 40.5	36.9 ± 8.3	3.8 ± 0.8		50.7 ± 6.2	25.8 ± 6.9	110.4 ± 8.9	1.10 ± 0.7		
54.8	188.8 ± 19.8	105.2 ± 10.1	9.6 ± 1.1		272.2 ± 22.8	17.2 ± 4.3	186.4 ± 14.3	16.8 ± 1.4		
57.2	197.9 ± 29.0	108.6 ± 12.2	12.7 ± 1.5		298.4 ± 25.5	— —	150.0 ± 11.6	29.8 ± 2.1		
60.9	108.1 ± 11.7	213.2 ± 18.1	16.4 ± 1.6		680.7 ± 52.6	7.9 ± 2.2	201.8 ± 15.7	88.8 ± 5.6		
63.1	161.9 ± 25.8	239.1 ± 22.0	16.0 ± 1.9		752.2 ± 57.8	15.9 ± 4.5	176.4 ± 13.9	126.5 ± 8.4		
66.6	38.0 ± 4.4	193.2 ± 16.7	14.3 ± 1.5	6.6 ± 2.0	850.6 ± 62.0	13.4 ± 4.3	147.4 ± 11.9	163.6 ± 8.1	0.4 ± 0.1	3.3 ± 1.0
68.5	46.8 ± 9.0	163.1 ± 17.3	11.8 ± 1.6	14.7 ± 8.3	742.1 ± 60.9	18.6 ± 5.4	121.3 ± 10.0	183.4 ± 9.3	4.6 ± 0.6	5.4 ± 1.1
73.7	15.7 ± 2.8	137.2 ± 15.4	9.7 ± 1.4	24.2 ± 3.3	638.2 ± 51.8	40.6 ± 10.2	92.4 ± 8.1	255.7 ± 13.6	18.6 ± 2.1	19.7 ± 2.2

reactions. It calculates compound nuclear decay following width fluctuation theory, which correlates the incident and exit channels with width fluctuation up to 3.00 MeV. The essential improvement in cluster emissions has been interpreted by Iwamoto-Harada calculations for PEQ. The input parametrization including nuclear masses, fission barriers, discrete levels transitions, γ strength functions, optical model parameters and Kalbach systematics angular distributions are internally selected by RIPL-3 [46]. The level densities are selected by phenomenological Gilbert-Cameron model (GC) [47], generalized superfluid model (GSM) [48], enhanced generalized superfluid model (EGSM) [49] with corresponding parametrizations. The GC approach separates the applicability of the excitation energy into constant temperature formula and Fermi gas formula but it does not account explicitly for the collective enhancements of the level densities. The GSM describes the superfluid behavior of the nucleus at the low-energy region to the Fermi-Gas model at the high-energy region during the phase transition. However, the empire global specific model (EGSM) includes the superfluid model and the Fermi gas model below and above critical excitation energy, respectively. It includes an accurate treatment for spin distribution and high angular momenta for the heavy-ion reaction. In the case of GC, three systematics are incorporated in terms of level density parameter, $\tilde{a}$, and the shell effect parameter, $\bar{\gamma}$; Ignatyuk *et al.*: $\tilde{a} = 0.154A+(6.3\times\ 10^{-5})A^2$ and $\bar{\gamma} = -0.054$, Arthur: $\tilde{a} = 0.1375A-(8.36\times10^{-5})A^2$, and $\bar{\gamma} = -0.054$, Iljinov *et al.*: $\tilde{a} = 0.114A+(9.80\times10^{-2})A^{2/3}$ and $\bar{\gamma} = -0.051$. In GSM, the asymptotic value of a-parameter $\tilde{a}$ is assumed as $\tilde{a} = \alpha A+\beta A^{2/3}$, $\bar{\gamma} = \gamma_0 A^{1/3}$ where $\alpha = 0.103$, $\beta = -0.105$, and $\gamma_0 = 0.375$ is obtained using Myers-Swiatecki correction along with deformation term. The effective excitation energy (U in MeV) in EGSM is associated to the excitation energy (E_x) by $U = E_x+n\triangle_o$, where $\triangle_o=12/\sqrt{A}$ is termed as the average correlation function of the ground state, n= 0, 1, and 2 for even-even, odd-A and odd-odd nuclei, receptively. The resulting EGSM systematics is adopted by the set of parameters $\alpha = 0.0748$, $\beta = 0.00$, and $\gamma_0 = 0.5609$.

B. Production of evaporation residues

Quantitative measurement of the radionuclides produced in the ^{12}C-induced reaction on the ^{89}Y was accomplished within the 3.3–6.3 MeV/nucleon energy range. A typical γ-ray spectrum of the residues produced in the ^{12}C+^{89}Y reaction at 73.7 MeV, collected after 38 min of the EOB, is reported in Fig. 1. The production of ^{98,97g,97m,96}Rh, ^{97}Ru, ^{96,95,94,93}Tc, and ^{93m}Mo in the target matrix is shown in the spectrum by their characteristic γ rays. The nuclear spectroscopic data of the residues produced through various channels along with the reaction threshold are listed in Table I. The measured residual cross-section data at various incident energies are reported in Table II. A comparative analysis between the measured excitation functions of the residues and the theoretical model calculations are shown in Figs. 2, 5–7. The measured cross-sections are represented by symbols with uncertainty, and the theoretical estimations are indicated by curves in the figures.

1. Rh *isotopes:* $^{98,97g+m,96}$Tc

Figures 2(a)–2(d) depict the comparison of the measured cross-sections of $^{98,97m+g,96}$Rh and theoretical estimations from PACE4, which considers HF model for the EQ process,

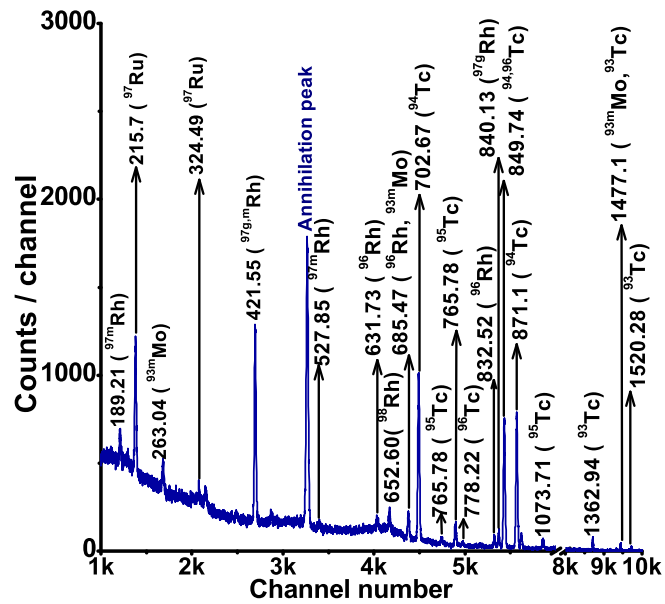

FIG. 1. A γ-ray spectrum of 73.7 MeV ^{12}C activated ^{89}Y collected after 38 min of the EOB.

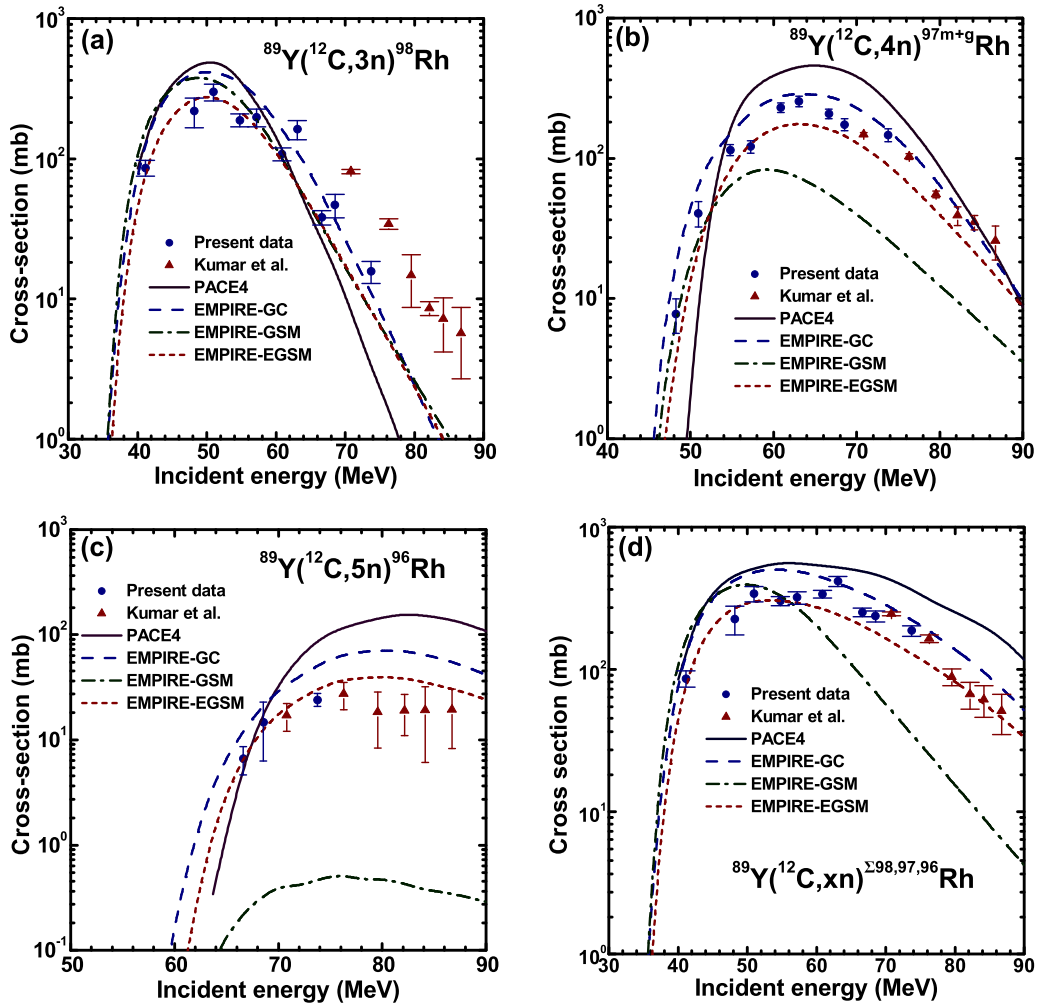

FIG. 2. Comparison of experimental cross-sections of (a) ^{98}Rh, (b) $^{97m+g}$Rh, (c) ^{96}Rh, and (d) $^{98+97(m+g)+96}$Rh from the ^{12}C+^{89}Y reaction with the theoretical estimations.

and EMPIRE 3.2.2, which accounts for the HF and EM models for EQ and PEQ processes, respectively, within the energy range, ∼40–90 MeV. The measured cross-sections of ^{98}Rh have been compared with the theoretical estimations with different level densities: GC, GSM, and EGSM in Fig. 2(a).

The cross-sections of ^{98}Rh are in good agreement with the EMPIRE estimations, particularly with the EGSM-level density throughout the energy range. It is also observed that both the measurements follow a smooth decreasing trend in cross-section with increasing energies; however, the present measurement is almost half of the cross-sections reported by Kumar *et al.* [31] at the overlapping energies. The observed difference might be due to the variation of the off-line counting statistics because of the very short half-life (8.72 min) of ^{98}Rh. Nevertheless, a clear indication of PEQ emission of neutrons is observed in the 3*n* channel at the high-energy tail (∼60–87 MeV) of the measured excitation functions where PACE4 calculations largely underpredict the data.

Unlike the measurement in Ref. [31] that reports only ^{97}Rh, the production of the isomeric and ground state of ^{97}Rh has been confirmed from the analysis of decay data and they are also indicated in Fig. 1. The sum of isomeric and ground state cross-sections, $^{97m+g}$Rh, are compared with the estimations from the PACE4 with GC-level density, and EMPIRE with GC/GSM/EGSM, as shown in Fig. 2(b). The reported cross-sections of ^{97}Rh [31] are also shown in Fig. 2(b) and they seem to follow the trend of the present measurement satisfactorily. It is observed that the measured cross-sections are well reproduced by the EMPIRE with GC/EGSM-level density, while PACE largely underestimates the data at the low-energy range and overpredicts them at the high energies.

Similarly, it compares the cross-sections of ^{96}Rh produced through the 5*n* reaction channel with the theoretical estimations Fig. 2(c). The experimental data agree well with the EMPIRE estimations with EGSM within ∼66–78 MeV beyond which it overpredicts the data. The similar calculations with GC- and GSM-level densities largely overpredict and underpredict the data throughout the energy range, respectively. Grossly, the cross-sections of ^{96}Rh are overpredicted by PACE4.

In Fig. 2(d), the total experimental cross-sections of the *xn* channels, i.e., the sum of cross-sections of ^{98,97g,97m,96}Rh, are compared with the theory. The total cross-sections lie between the EMPIRE estimations with GC and EGSM following the

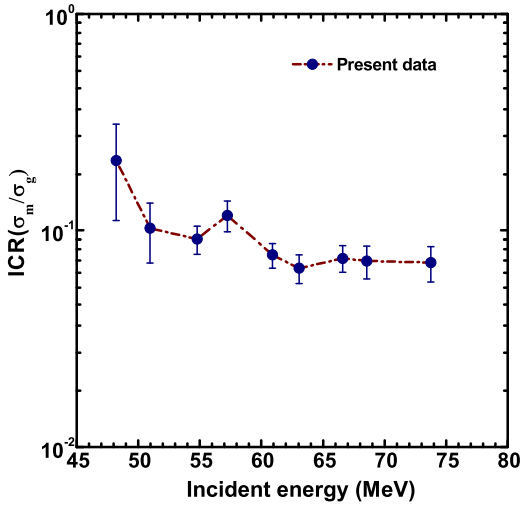

FIG. 3. Variation of ICR of ^{97}Rh at different bombarding energies.

trend, while the same with GSM grossly underestimates the data beyond 55 MeV, and PACE4 overpredicts the data throughout the range.

Since isomeric and ground state cross-sections of ^{97}Rh have been measured in the present study, isomeric cross-section ratio (ICR), which is defined as the cross-section ratio of the low-spin state ^{97m}Rh ($1/2^-$) to the high-spin state ^{97g}Rh ($9/2^+$), has been estimated at different incident energies in the range ∼40–75 MeV (Fig. 3). The ICRs vary between 0.21 and 0.07. The ICR decreases initially with increasing incident energy and becomes almost constant above 60 MeV energy. This observation agrees with the fact that the fusion of ^{12}C projectile in ^{89}Y leads to the formation of compound nucleus, ^{101}Rh, at the high spin state, which preferentially decays to the high spin state of ^{97}Rh through the 4n channel at relatively lower bombarding energies leading to the decrease in ICR values. However, with the considerable increase in the bombarding energy, the population of the low-spin metastable state of ^{97}Rh increases and that justifies the constant ICRs above 60 MeV energy. A similar trend in ICRs of ^{99}Rh was observed in the fusion of ^{12}C in ^{89}Y at the subbarrier and near barrier energies [50].

2. ^{97}Ru: *A cumulative estimation*

Production of ^{97}Ru may follow two pathways:

(a) the complete fusion of ^{12}C in ^{89}Y leads to the production of ^{97}Ru through the $p3n$ channel:

$$^{12}\mathrm{C} + ^{89}\mathrm{Y} \rightarrow [^{101}\mathrm{Rh}]^* \rightarrow ^{97}\mathrm{Ru} + p3n, \quad Q = -33.1\,\mathrm{MeV}; \tag{3}$$

(b) decay from its precursor ^{97}Rh: the fusion of ^{12}C in ^{89}Y leads to the production of ^{97g}Rh and ^{97m}Rh through 4n channel. Since the half-lives of ^{97g}Rh and ^{97m}Rh are short, 30.7 and 46.2 min, respectively, they decay to relatively long-lived ^{97}Ru (2.83 d). The radionuclide ^{97g}Rh decays to ^{97}Ru through $\epsilon + \beta^+$ (100%) mode, and ^{97m}Rh decays to ^{97}Ru through $\epsilon + \beta^+$ (94.4%) and IT (5.6%):

$$^{12}\mathrm{C} + ^{89}\mathrm{Y} \rightarrow [^{101}\mathrm{Rh}]^* \rightarrow ^{97g}\mathrm{Rh}/^{97m}\mathrm{Rh} + 4n\ (Q = -37.4\,\mathrm{MeV}),$$
$$^{97g}\mathrm{Rh}(\epsilon + \beta^+) \rightarrow ^{97}\mathrm{Ru},$$
$$^{97m}\mathrm{Rh}(\epsilon + \beta^+ \,\&\, \mathrm{IT}) \rightarrow ^{97}\mathrm{Ru}. \tag{4}$$

A simplified decay scheme of ^{97g}Rh and ^{97m}Rh that populates ^{97}Ru has been shown in Fig 4. Thus, the cross-sections of ^{97}Ru are contributed by the direct reaction channel and indirectly through the decay of ^{97g}Rh and ^{97m}Rh.

The measured cumulative cross-section of ^{97}Ru within 40–75 energy range has been compared with theoretical cross-sections of ^{97}Ru, $^{97m+g}$Rh, and the total of $^{97m+g}$Rh+^{97}Ru, obtained from EMPIRE with GC-level density as shown in Fig. 5. Since model calculation considers only the direct pathways for the production of residues, estimated theoretical cross-sections of ^{97}Ru and $^{97m+g}$Rh individually underpredict the measured data; however, an excellent reproduction of the measured cross-section has been observed when compared with the total theoretical cross-section, i.e., sum of the cross-sections of ^{97}Ru and $^{97m+g}$Rh above 58 MeV. The measured cross-sections of ^{97}Ru reported in Ref. [31] are also in good agreement with the total theoretical cross-sections in the 70–87 MeV range. Thus, the cumulative cross-section of ^{97}Ru is well reproduced by the EMPIRE estimation with GC-level density over a wide range 55–87 MeV. At the lower energies (< 58 MeV), cumulative cross-sections of ^{97}Ru are better reproduced by the individual theoretical cross-sections of $^{97m+g}$Rh, and ^{97}Ru with no considerable difference in values. The maximum cross-section of ^{97}Ru was found to be ∼850 mb at 66.6 MeV. Due to the large effective cross-section, ^{97}Ru could be produced in a considerable quantity for the application purpose.

Since the half-life of daughter radionuclide, ^{97}Ru, is much greater than its precursors, ^{97g,m}Rh, the independent production cross-section of ^{97}Ru, could be estimated following the prescription of Cavinato *et al.* [24] as given below:

$$\sigma^i = \sigma^c - \sigma^p \left[\frac{T^d_{1/2}}{T^d_{1/2} - T^p_{1/2}}\right] P^p, \tag{5}$$

where σ^i, σ^c represent the independent and cumulative cross-sections of daughter, respectively; σ^p is the independent production cross-section of the precursor radionuclide; P^p represents the branching ratio of precursor radionuclide and $T^p_{1/2}$ and $T^d_{1/2}$ are the half-lives of precursor and daughter radionuclides, respectively. Therefore, the independent production of ^{97}Ru is given by

$$\sigma^i_{^{97}\mathrm{Ru}} = \sigma^c_{^{97}\mathrm{Ru}} - 1.0075 \times \left(\sigma^p_{^{97}\mathrm{Rh}} P^p\right). \tag{6}$$

A comparison between the derived excitation function for the independent production of ^{97}Ru from the ^{89}Y(^{12}C, $p3n$)^{97}Ru reaction is also shown in Fig. 5. The estimated independent excitation function of ^{97}Ru is well described by EMPIRE, while PACE4 underpredicts them throughout the range. The independent cross-sections of ^{97}Ru through $p3n$

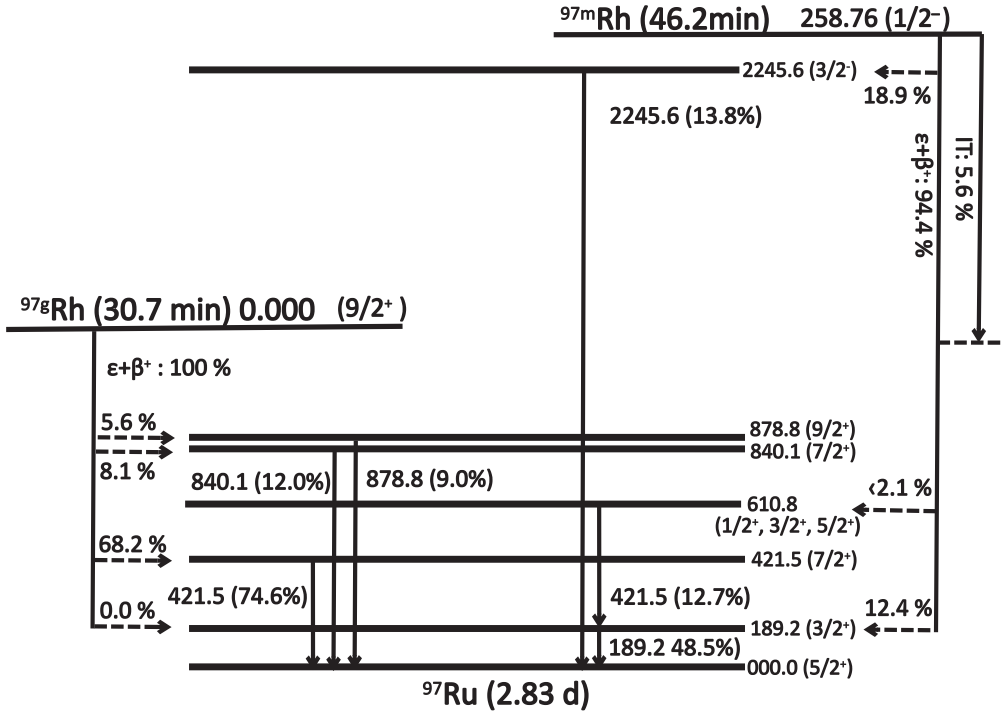

FIG. 4. Simplified decay scheme of ^{97g}Rh and ^{97m}Rh into ^{97}Ru.

channel were found to be ∼640 mb at 66.6 MeV bombarding energy.

3. Tc *isotopes:* ^{96,95,94,93}Tc

The cross-sections of ^{96,95,94,93}Tc isotopes populated from the excited compound nucleus are plotted in Figs. 6(a)–6(d) and are compared with the theoretical estimations within 40–87 MeV energy range.

The production of ^{96}Tc through αn channel is shown in Fig. 6(a). It is observed that the trend of measured cross-sections of ^{96}Tc is well reproduced by the EMPIRE estimation

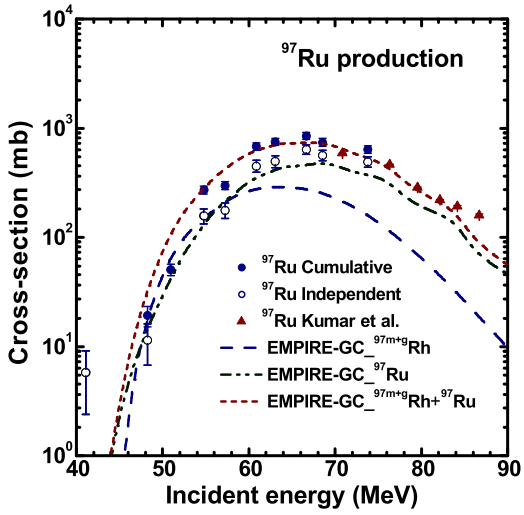

FIG. 5. Comparison of cumulative ($^{97m+g}$Rh+^{97}Ru) and independent cross-sections of ^{97}Ru from ^{12}C+^{89}Y reaction with the EMPIRE3.2.2 estimations.

with different level density options, a decent match between the cross-section values measured in the present experiment and those reported in Ref. [31] in the overlapping energy region is also observed. More precisely, the HF-EM calculation with EGSM-level density better reproduces the measured cross-sections up to ∼67 MeV, and it underestimates them above it.

Similarly, in Fig. 6(b), EMPIRE calculation with GSM-level density reproduces the experimental excitation function of ^{95}Tc well up to ∼75 MeV, while two other calculations with GC- and EGSM-level densities underpredict the data. The reported data in Ref. [31] shows an incongruent trend and ∼55% higher cross-section values around ∼75 MeV compared to the EMPIRE with GSM. However, PACE4 estimations are grossly lower compared to the measured data of ^{95}Tc and ^{96}Tc throughout the energy range. The experimental excitation function of ^{94}Tc is found consistent with the EMPIRE estimations, and PACE4 within the experimental range with a faint indication of enhanced cross-section beyond 70 MeV in our data, although the previous measurement deviates between 70–87 MeV as shown in Fig. 6(c).

Figure 6(d) shows the production of the ^{93}Tc through the $\alpha 4n$ channel from the complete fusion of ^{12}C with ^{89}Y. The experimental excitation function is moderately reproduced by the HF estimations with EGSM-level density with slight overprediction at the high energies, while PACE4 crudely overpredicts the data throughout the range. The EMPIRE estimation with GC also shows a large overprediction up to ∼80 MeV, while EMPIRE with GSM-level density badly fails to reproduce the experimental cross-sections.

In Fig. 7(a), the total cross-sections of αxn channels have been compared. EMPIRE calculation with EGSM and GSM reproduces the experimental cross-sections fairly well

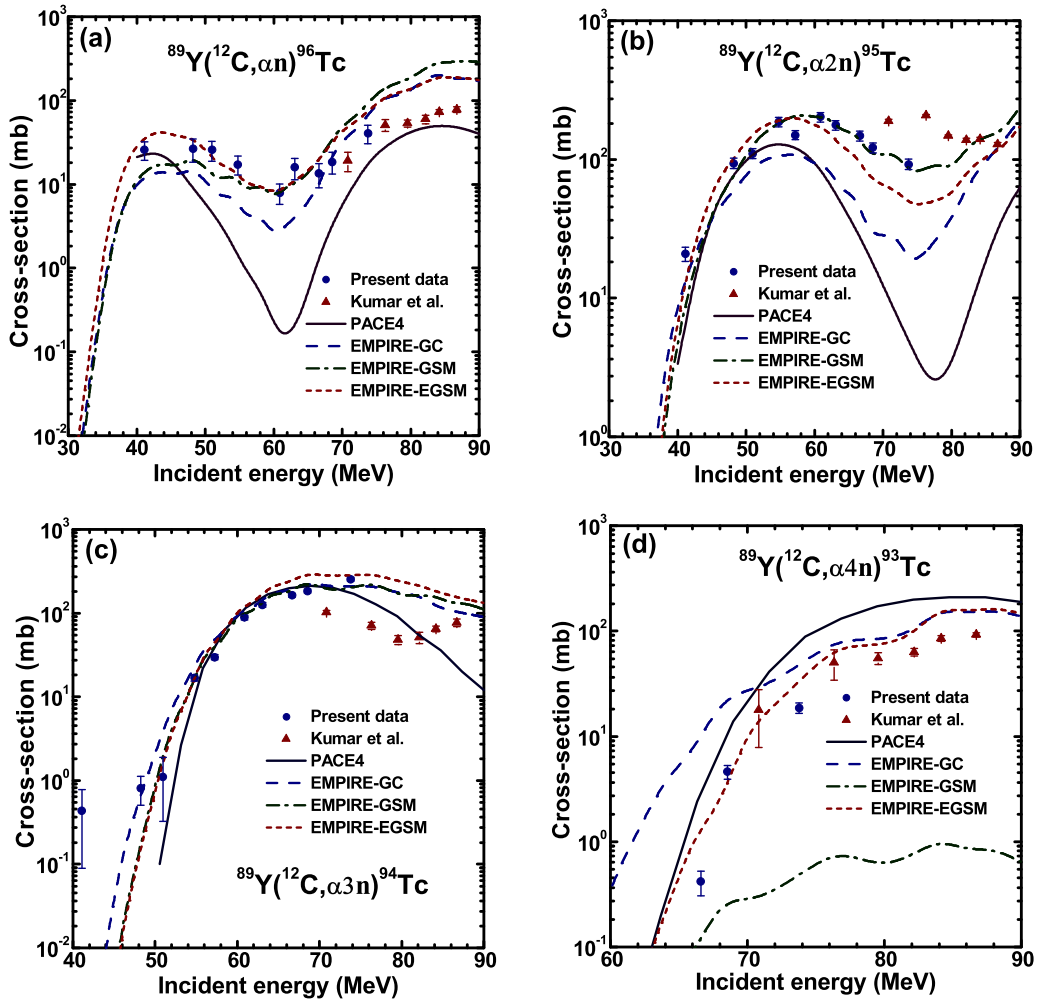

FIG. 6. Comparison of experimental excitation functions of (a) ^{96}Tc, (b) ^{95}Tc, (c) ^{94}Tc, and (d) ^{93}Tc with the theoretical estimations.

compared to the GC-level density; however, the trend of experimental values is well reproduced by PACE4, although it mostly underpredicts the total cross-section.

4. Mo *isotope:* ^{93m}Mo

The measured excitation functions of ^{93m}Mo has been compared with the EMPIRE calculations as shown in Fig. 7(b).

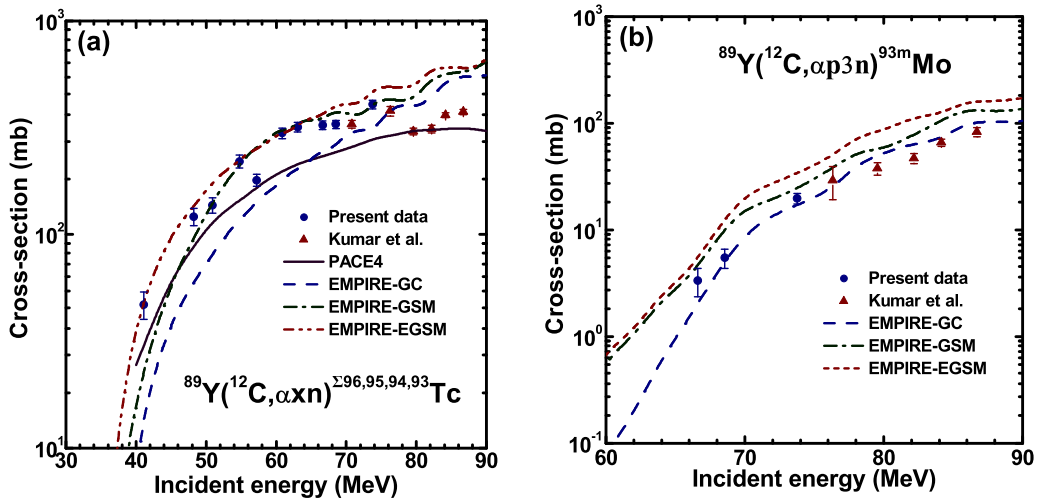

FIG. 7. (a) Same as described in the caption of Fig. 6 for $^{96+95+94+93}$Tc. (b) Comparison of experimental excitation functions of ^{93m}Mo with EMPIRE3.2.2.

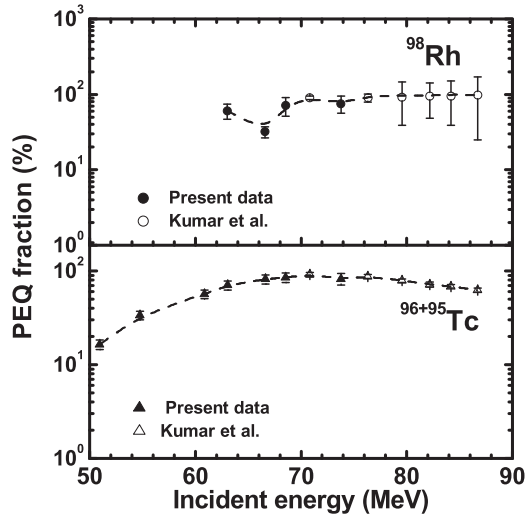

FIG. 8. Variation of PEQ fraction for $3n$ and $\alpha n+\alpha 2n$ channels.

The experimental cross-sections are well reproduced by the GC-level density, whereas two other level densities, GSM and EGSM, slightly overestimate the data. It is evident that the present measurement of cross-section satisfactorily follows the trend of the cross-sections reported in Ref. [31] within the 70–87 MeV range. The production of ^{93m}Mo is assumed through the $\alpha p3n$ channel as the possibility through the $3p5n$ channel is limited by threshold energy of 71.6 MeV.

Although a clear difference is observed between various level densities used in the EMPIRE, and no single level density could explain all the residues satisfactorily, the overall performance of EMPIRE is fairly acceptable in reproducing the measured data compared to the PACE4.

5. Preequilibrium fraction

The residual cross-sections measured from the ^{12}C+^{89}Y reaction are analyzed using the EQ and PEQ models. EMPIRE uses HF and EM models for the estimation of EQ and PEQ reactions, while PACE4 is based on the HF model, accounting only for the EQ reactions.

Since a sizable enhancement in cross-sections is observed for ^{98}Rh, ^{96}Tc, and ^{95}Tc produced by the $3n$, αn, and $\alpha 2n$ channel, respectively, above 60 MeV compared to the estimation of PACE4, the difference in cross-sections at a given energy could be attributed to the PEQ processes. The cross-sections of those radionuclides reported in Ref. [31] at even higher energies (70–87 MeV) were found to be consistent with the present measurement and EMPIRE estimations. To understand the strength of the PEQ process, PEQ fraction has been calculated for the $3n$ and $\alpha n+\alpha 2n$ channel over a wide range, ∼48–87 MeV. The variation of PEQ fraction is shown in Fig. 8. PEQ fraction increases with increasing projectile energy and reaches a saturation value beyond threshold energy, above which the PEQ process dominates over EQ.

IV. CONCLUSION

This article reports the new cross-sections of the residual radionuclides produced in the ^{12}C+^{89}Y reaction in the 40–75 MeV energy and the data have been analyzed using theoretical model calculations from HF and EM models in the framework of PACE4 and EMPIRE3.2.2 with different level density models/parameters. Though the experimental and theoretical cross-sections differ for some radionuclides, the overall analysis indicates that the compound nuclear process is a predominant mechanism in the 40–75 MeV energy range, although the signature of PEQ process is observed in few cases such as $3n$, αn, and $\alpha 2n$ channels.

The cumulative cross-sections of ^{97}Ru agree well with the sum of theoretical cross-sections of ^{97m}Rh, ^{97g}Rh, and ^{97}Ru produced through the ^{89}Y (^{12}C,4n) and ^{89}Y(^{12}C,p3n) channels, respectively. It is evident that several other radionuclides will also be produced in the same energy region, however, many of them are short-lived, except ^{96,95}Tc, or have negligible production. Since the maximum cross-section of ^{97}Ru is found to be 850 mb at 66.6 MeV, which is substantial, the route could be used to produce ^{97}Ru in the no-carrier-added form provided that the Ru is separated from the bulk Y and coproduced Tc and Mo radionuclides [13–15] for the small-scale applications. This article is informative for the optimization of production parameters of ^{97}Ru radionuclides and also to understand the reliability of the theoretical models.

ACKNOWLEDGMENTS

We thank the Pelletron staff of the BARC-TIFR Pelletron facility for their cooperation during the experiment. Research Grant No. CRG/2018/002354 from SERB, Government of India, is gratefully acknowledged. The fellowship from MHRD, Government of India, is acknowledged by A.C.

[1] S. C. Srivastava, P. Som, G. Meinken, A. Sewatkar, and T. H. Ku, Brookhaven National Laboratory, Report No. BNL 24614 (1978).
[2] D. Comar and C. Crouzel, Radiochem. Radioa. Let. **27**, 307 (1976).
[3] F. H. Deland, A. E. James, Jr., H. N. Wagner, Jr., and F. Hosain, J. Nucl. Med. **12**, 683 (1971).
[4] P. Som, F. Hosain, H. N. Wagner, Jr., and U. Scheffel, J. Nucl. Med. **13**, 551 (1972).
[5] M. M. Vora, Appl. Radiat. Isotopes **42**, 19 (1991).
[6] Z. H. Oster, P. Som, M. C. Gil, R. G. Fairchild, A. G. Goldman, E. R. Schachner, D. F. Sacker, H. L. Atkins, G. E. Meinken, S. C. Srivsatava, P. Richards, and A. B. Brill, J. Nucl. Med. **22**, 269 (1981).
[7] E. R. Schachner, M. C. Gil, H. L. Atkins, P. Som, S. C. Srivastava, J. Badia, D. F. Sacker, R. G. Fairchild, and P. Richards, J. Nucl. Med. **22**, 352 (1981).
[8] M. C. Lagunas-Solar, M. J. Avila, N. J. Navarro, and P. C. Johnson, Int. J. Appl. Radiat. Isotopes **34**, 915 (1983).

[9] N. G. Zaitseva, V. I. Stegailov, V. A. Khalkin, N. G. Shakun, P. T. Shishlyannikov, and K. G. Bukov, Appl. Radiat. Isotopes **47**, 145 (1996).
[10] G. Comparetto and S. M. Qaim, Radiochim. Acta **27**, 177 (1980).
[11] P. J. Pao, J. L. Zhou, D. J. Silvester, and S. L. Waters, Radiochem. Radioa. Let. **46**, 21 (1981).
[12] M. Maiti and S. Lahiri, Radiochim. Acta **99**, 359 (2011).
[13] M. Maiti, Radiochim. Acta **101**, 437 (2013).
[14] M. Maiti and S. Lahiri, Radiochim. Acta **103**, 7 (2015).
[15] M. Maiti, A. Datta, and S. Lahiri, RSC Adv. **5**, 80919 (2015).
[16] D. Kumar, M. Maiti, and S. Lahiri, Sep. Sci. Technol. **52**, 2372 (2017).
[17] D. Kumar, M. Maiti, and S. Lahiri, Phys. Rev. C **94**, 044603 (2016).
[18] D. Kumar and M. Maiti, Phys. Rev. C **96**, 044624 (2017).
[19] D. Kumar, M. Maiti, and S. Lahiri, Phys. Rev. C **96**, 014617 (2017).
[20] D. Kumar and M. Maiti, Phys. Rev. C **95**, 064602 (2017).
[21] L. Westerberg, D. G. Sarantites, D. C. Hensley, R. A. Dayras, M. L. Halbert, and J. H. Barker, Phys. Rev. C **18**, 796 (1978).
[22] P. Vergani, E. Gadioli, E. Vaciago, E. Fabrici, E. Gadioli Erba, M. Galmarini, G. Ciavola, and C. Marchetta, Phys. Rev. C **48**, 1815 (1993).
[23] T. C. Awes, G. Poggi, C. K. Gelbke, B. B. Back, B. G. Glagola, H. Breuer, and V. E. Viola, Jr., Phys. Rev. C **24**, 89 (1981).
[24] M. Cavinato, E. Fabrici, E. Gadioli, E. Gadioli Erba, P. Vergani, M. Crippa, G. Colombo, I. Redaelli, and M. Ripamonti, Phys. Rev. C **52**, 2577 (1995).
[25] C. Birattari, M. Bonardi, M. Cavinato, E. Fabrici, E. Gadioli, E. Gadioli Erba, F. Groppi, M. Bello, C. Bovati, A. Di Filippo, T. G. Stevens, S. H. Connell, J. P. F. Sellschop, S. J. Mills, F. M. Nortier, G. F. Steyn, and C. Marchetta, Phys. Rev. **54**, 3051 (1996).
[26] M. K. Sharma, P. P. Singh, D. P. Singh, A. Yadav, V. R. Sharma, I. Bala, R. Kumar, Unnati, B. P. Singh, and R. Prasad, Phys. Rev. C **91**, 014603 (2015).
[27] R. Vandenbosch and J. R. Huizenga, Phys. Rev. **120**, 1313 (1960).
[28] M. J. A. De Voigt, K. Maeda, H. Ejiri, T. Shibata, K. Okada, T. Motobayashi, M. Sasao, T. Kishimoto, H. Suzuki, H. Sakai, and A Shimizu, Nucl. Phy. A **379**, 160 (1982).
[29] N. Chakravarty, P. K. Sarkar, and S. Ghosh, Phys. Rev. C **45**, 1171 (1992).
[30] S. Sudar and S. M. Qaim, Phys. Rev. C **53**, 2885 (1996).
[31] B. B. Kumar, S. Mukherjee, S. Chakrabarty, B. S. Tomar, A. Goswami, and S. B. Manohar, Phys. Rev. C **57**, 743 (1998).
[32] S. Mukherjee, A. Goswami, and B. S. Tomar, Phys. Rev. C **72**, 067602 (2005).
[33] J. F. Ziegler, J. Appl. Phys./ Rev. Appl. Phys. **85**, 1249 (1999).
[34] http://www.nndc.bnl.gov/nudat2/ (National Nuclear Data Center, Brookhaven National Laboratory).
[35] M. Maiti and S. Lahiri, Phys. Rev. C **84**, 067601 (2011).
[36] M. Maiti, Phys. Rev. C **84**, 044615 (2011).
[37] M. Maiti and S. Lahiri, Phys. Rev. C **81**, 024603 (2010).
[38] A. Chauhan and M. Maiti, Phys. Rev. C **99**, 034608 (2019).
[39] J. Kemmer and R. Hofmann, Nucl. Instrum. Methods **176**, 543 (1980).
[40] A. Gavron, Phys. Rev. C **21**, 230 (1980).
[41] H. Feshbach, A. Kerman, and S. Koonin, Ann. Phys-New York **125**, 429 (1980).
[42] R. Bass, Phys. Rev. Lett. **39**, 265 (1977).
[43] C. A. Engelbrecht and H. A. Weidenmuller, Phys. Rev. C **8**, 859 (1973).
[44] C. K. Cline, Nucl. Phys. A **193**, 417 (1972).
[45] I. Ribansky, P. Oblozinsky, and E. Betak, Nucl. Phys. A **205**, 545 (1973).
[46] R. Capote, M. Herman, P. Oblozinsky, P. G. Young, S. Goriely, T. Belgya, A. V. Ignatyuk, A. J. Koning, S. Hilaire, V. A. Plujko, M. Avrigeanu, O. Bersillon, M. B. Chadwick, T. Fukahori, Zhigang Ge, Yinlu Han, S. Kailas, J. Kopecky, V. M. Maslov, G. Reffo, M. Sin, E. Sh. Soukhovitskii, and P. Talou, Nucl. Data Sheets **110**, 3107 (2009).
[47] A. Gilbert and A. G. W. Cameron, Can. J. Phys. **43**, 1446 (1965).
[48] A. V. Ignatyuk, J. L. Weil, S. Raman, and S. Kahane, Phys. Rev. C **47**, 1504 (1993).
[49] V. A. Plujko, O. M. Gorbachenko, B. M. Bondar, and E. P. Rovenskykh, Nucl. Data Sheets **118**, 240 (2014).
[50] S. Mukherjee, N. L. Singh, G. K. Kumar, and L. Chaturvedi, Phys. Rev. C **72**, 014609 (2005).